



FATIGUE AND FRACTURE OF ADDITIVELY MANUFACTURED MATERIALS

Evaluating Molybdenum-Rhenium Alloys Through Additive Manufacturing

CAYLA C. ECKLEY,¹ RYAN X. KINKADE,¹ BRIANNA M. SEXTON,¹
TRAVIS E. SHELTON,¹ CHRISTINE SCHUBERT-KABBAN,²
CARL R. HARTSFIELD,¹ JOHN S. BREWER,¹ and RYAN A. KEMNITZ^{1,3}

1.—Department of Aeronautics and Astronautics, Air Force Institute of Technology, Dayton OH 45433, USA. 2.—Department of Mathematics, Air Force Institute of Technology, Dayton OH 45433, USA. 3.—e-mail: Ryan.Kemnitz@afit.edu

Highly successful advanced manufacturing techniques of refractory metals are becoming increasingly necessary to navigate technology gaps. Refractory metal alloys are desirable to meet the need for high temperature structural materials, but are difficult to produce because of their high strength, low ductility, and high melting point. This work demonstrates the use of laser powder bed fusion to produce several Mo-Re alloys by additively manufacturing mechanically mixed pure elemental powders. Relationships are explored between mechanical properties regarding build orientation, laser speed, rhenium alloy content, and the addition of 3% hydrogen to the argon shield gas. Mechanical characterization was accomplished by three-point flexural testing. Rhenium content, hydrogen addition to the shield gas, and build orientation were all found to significantly affect the flexural strength. The build direction had the highest influence, and a maximum strength of 833.3 MPa was achieved in the vertical direction while the maximum strength in the horizontal direction was 346.1 MPa.

INTRODUCTION

Molybdenum is a refractory metal which possesses a high melting point, high thermal and electrical conductivity, and exceptional resistance to wear and corrosion. These properties make the metal and its alloys useful for high-temperature structural applications but also difficult to manufacture. The layer-by-layer process of additive manufacturing (AM) makes it possible to synthesize complex geometries that would be labor-intensive or impossible to produce by traditional means. Despite its noted benefits over traditional manufacturing, laser powder bed fusion (LPBF) presents unique challenges that must be overcome to achieve dense, strong molybdenum. The behavior of molybdenum

following the AM process has been the subject of many studies with focuses on porosity, impurity segregation, and crystallographic texture of manufactured parts.^{1–6} Molybdenum exhibits a brittleness inherent to the material, with grain boundaries serving as crack facilitators and propagators.^{7–9} As a result, pure molybdenum manufactured by LPBF frequently suffers from high porosity and displays undesirable intergranular fracture behavior.^{5,10}

A common method to improve the mechanical properties of traditionally manufactured molybdenum is by alloying with rhenium. Rhenium is soluble in molybdenum up to 50 wt.% and has been shown to improve both low and high temperature mechanical properties of the material.^{11,12} The mechanism underlying this beneficial effect is not precisely known, but it has been suggested that rhenium promotes the formation of twin boundaries which in turn facilitate more deformation in the material.¹¹ Alloy softening at low temperatures with small additions of rhenium has also been observed in many BCC metals, including molybdenum.¹³ Although the benefit of alloying with

The views expressed in this article are those of the authors and do not reflect the official policy or position of the United States Air Force, Department of Defense, or the US Government.

(Received December 5, 2022; accepted March 20, 2023; published online April 7, 2023)

rhenium is well documented, the high cost of rhenium is a major factor to consider, and its use is cost prohibitive for some applications. It is worthwhile to explore dilute rhenium solute concentrations with the goal of balancing cost with the beneficial effect of rhenium.

Another method of improving refractory metals manufactured by LPBF is to modify the gas under which the process is carried out. Argon is commonly used to minimize the presence of oxygen and prevent chemical reactions during the melting process, but trace amounts of oxygen remain in the build environment. In their review of AM tungsten studies, Morcos et al. found that oxygen presence in the build chamber, when reported, ranged from 10 to 1000 ppm.¹⁴ Like all refractory metals, molybdenum has a high affinity for oxygen at elevated temperatures, and even small amounts of oxygen can have detrimental effects on grain boundary strength and layer wettability.¹⁵ Recent studies have demonstrated grain refinement and improvements in mechanical strength when adding a small amount of hydrogen to the argon process gas.¹⁶ This study utilized the same argon-hydrogen shield gas mixture to test whether the effect observed on pure metal is also helpful with alloys. The atmosphere of argon-3% hydrogen gas was chosen to avoid flammability of the gas.¹⁷⁻¹⁹

In the present study, the combined effect of alloying with rhenium and printing in an argon-3% hydrogen gas environment was studied in the low-temperature mechanical performance of additively manufactured molybdenum. Compositions of Mo-5wt.%Re, Mo-10wt.%Re, and Mo-25wt.%Re were printed in both inert argon and argon-3% hydrogen gas atmospheres. Although the solubility of rhenium in molybdenum allows for up to approximately 50 wt.% rhenium, the compositions in this present work were selected to study the effects of dilute amounts of rhenium in AM-produced alloys. Specimens were analyzed and compared based on chemical composition, room temperature flexural strength, and fracture mode.

MATERIALS AND METHODOLOGY

Materials

Pure molybdenum powder, 45 μm sieve, was manufactured by Tekna (Canada) using plasma atomization, and pure rhenium powder, 20 μm sieve, was manufactured by Rhenium Alloys, Inc. (USA). Powder mixtures of Mo-5wt.%Re, Mo-10wt.%Re, and Mo-25wt.%Re were made using a FlackTek (USA) DAC 250.1 FVZ-K SpeedMixer. Chemical composition analysis was performed on the pristine powders via inert gas fusion in a LECO ONH 836 machine at Luvak Inc. (USA). Scanning electron microscopy (SEM) images of the powders are shown in Fig. 1, and the oxygen content is reported in Table II.

All specimens were manufactured with a Concept Laser (Germany) Mlab Cusing 200R 3D metal printer equipped with a 50 μm diameter, 200 W continuous wave fiber laser. Specimens were printed using 200 W laser power, 20 μm layer height, 50 μm hatch spacing, and laser scanning speeds varying from 200–1000 mm/s. All specimens were manufactured using a meandering laser scanning strategy. Specimens were removed from the copper substrate by electrical discharge machining with a 0.5 mm offset. Three-point flexural specimens measuring 18 mm \times 4 mm \times 2 mm were manufactured on a pure copper build plate with build orientations perpendicular and parallel to the build plate, which are referred to as vertical and horizontal, respectively. Specimens of a similar size were reported on by Yin et al.²⁰ and this group.¹⁶ The orientations are visualized in Fig. 1. Printing atmospheres of argon and argon-3% hydrogen were used to minimize oxygen in the build chamber to < 1000 ppm, the lowest amount observable by the LPBF machine.

Energy-dispersive x-ray spectroscopy (EDS) maps were taken of the printed Mo-Re mixtures in each atmosphere to confirm the desired compositions were achieved and to analyze the homogeneity of the printed mixtures. Representative maps are displayed in Fig. 2.

Characterization

After manufacturing, the specimens were prepared for characterization. The sides of the specimens were ground and polished to remove surface texture inherent to the LPBF process to minimize the impact of surface porosity and cracking on the mechanical results. Specimen preparation was performed with a Buehler (USA) EcoMet 300. The specimens were then subjected to three-point flexural testing using an MTS (USA) Acumen 3 Electrodynamic Test System following the procedure outlined in ASTM E290. The specimens were tested until fracture.

Following fracture, specimens underwent fractographic analysis with a Tescan (Czech Republic) Maia-3 Field emission SEM. Electron backscatter diffraction (EBSD) maps were collected on specimens using an EDAX (USA) detector. Three maps were acquired for pure Mo, Mo-5%Re, Mo-10%Re, and Mo-25%Re printed with 200 mm/s in both argon and argon-3%hydrogen. An SEM accelerating voltage of 18 kV and beam intensity of 18 were used during map generation and specimens were tilted at 70° relative to the electron beam. EDAX orientation imaging microscopy (OIM) analysis software was used to perform grain size analysis. Reported grain size was obtained by averaging the data from three EBSD maps for each sample. Select specimens were etched with 30% hydrogen peroxide and analyzed via optical microscopy.

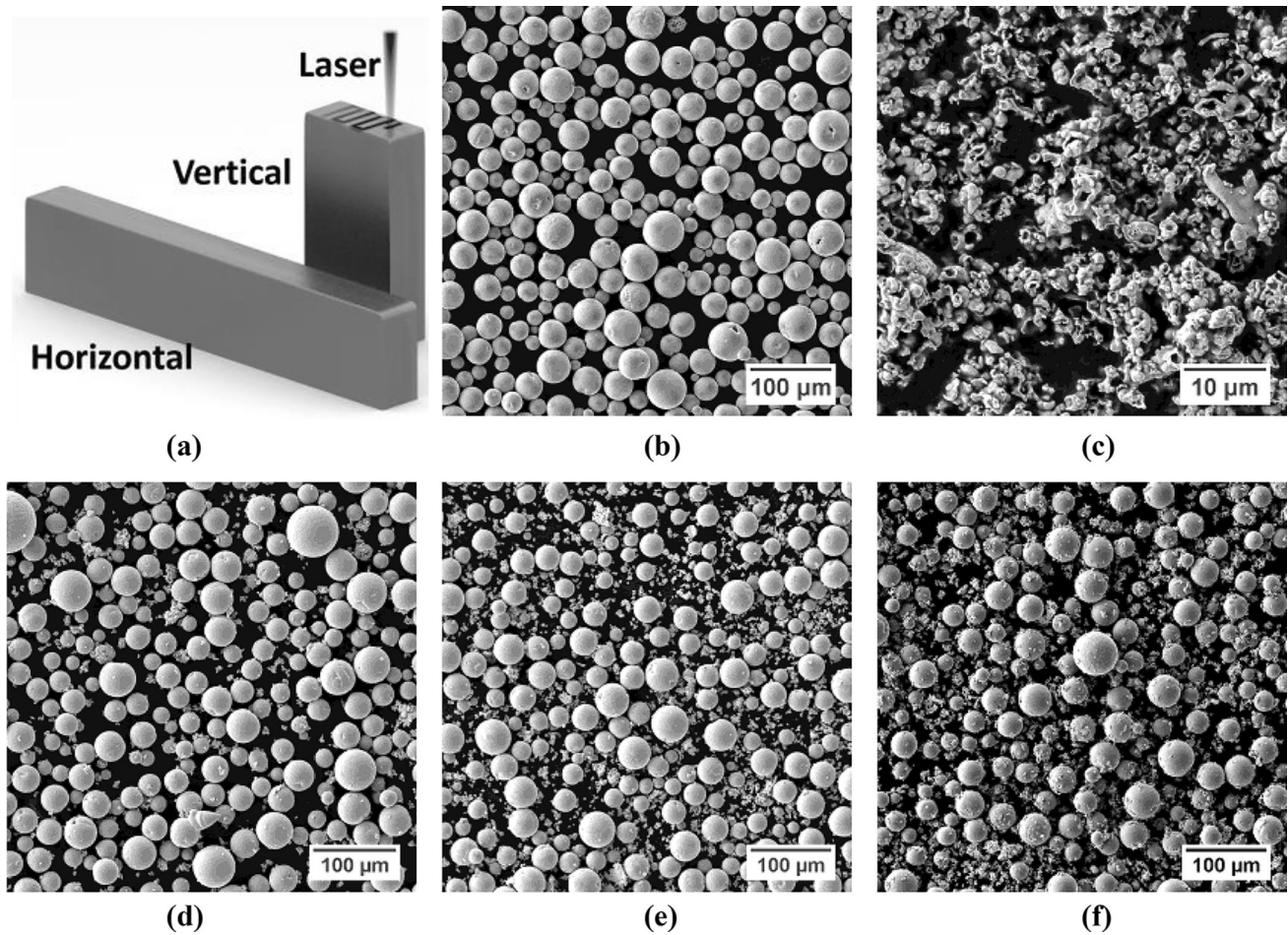


Fig. 1. Rendering of the LPBF process and its interaction with the material. Specifically, experimental beams were processed in a horizontal and vertical manner (a). Molybdenum (b), rhenium (c), Mo-5wt.%Re (d), Mo-10wt.%Re (e), and Mo-25wt.%Re (f) powders. Note the difference in scale between (c) and the other powder images.

Design of Experiments—Experimental Factors

To examine the performance impacts of these fabricated alloys we present a general, yet comprehensive design of experiments on the Mo-Re alloy strength in relation to processing parameters. The parameters chosen (Table I) and controlled include the build direction (horizontal or vertical), build atmosphere (Ar or Ar + H₂), alloy content (Mo, Mo-5wt.%Re, Mo-10wt.%Re, and Mo-25wt.%Re), and laser speed (200, 300, 400, 500, 600, 800, 1000 mm/s). A total of 327 specimens were successfully produced and subjected to mechanical testing for observation. Comparisons for each design parameter result in 112 (7 × 4 × 2 × 2) possible design settings, with 2–3 specimen replicates for each setting.

An initial full-factorial model was generated in JMP statistical software (USA), which significantly indicated the build direction having the strongest effect on strength. Therefore, the model was split into two separate models, one model for the horizontal and one for the vertical direction, which is

discussed throughout this article. Proceeding with results for each build direction provides finer detail for the other controlled variables while also providing an end-designer more knowledge on material and manufacturing limitations. Linearity was initially assumed, and parametric tests were conducted. All data obtained were plotted for further comparison and analyzed using an analysis of variance (ANOVA) to determine statistical significance. After model development, including the use of appropriate functional forms for the variables and the inclusion of important interaction terms, inferential procedures were used to determine whether the explanatory variables have effects on the response variable and, if so, the nature and magnitude of the effects.

RESULTS AND DISCUSSION

Chemistry and Microstructure

EDS maps of the printed material (Fig. 2) confirmed the desired compositions were achieved. Localized dark or bright areas in the maps indicate lower or high concentrations, respectively, of the

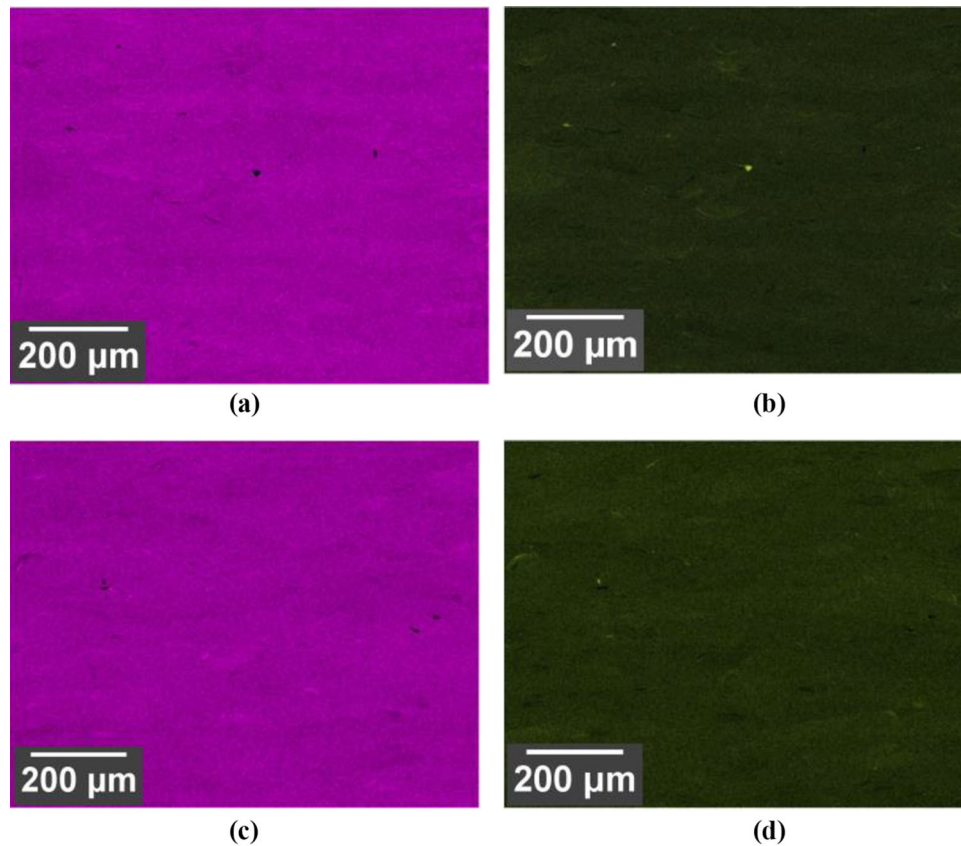


Fig. 2. EDS maps of as-built Mo-25Re printed in argon (a,b) and argon-3%hydrogen (c,d) showing the distribution of Mo in pink and Re in gray. All maps were taken in the XZ direction (Color figure online).

Table I. Experimental factors and levels

Parameter	Categorical level	Specific value
Build speed (mm/s)	–	200; 300; 400; 500; 600; 800; 1000
Alloy (wt.% Re)	–	Pure Mo; Mo-5%Re; Mo-10%Re; Mo-25%Re
Build direction (level)	1	Vertical
	0	Horizontal
Build environment (level)	1	Ar-H ₂ Mix
	0	Ar

displayed element relative to the rest of the image. Take note in Fig. 2b and d of the small bright spots, which indicate that small particles of rhenium were not completely incorporated into the molybdenum-rhenium matrix. These inhomogeneities were only found in the Mo-25wt.%Re specimens. We do not expect these small, unmixed particles to strongly affect the mechanical behavior of the Mo-Re alloys because rhenium is more ductile than molybdenum and its alloys. There was no observable difference in composition or mixing between the specimens printed in argon and argon-3%hydrogen.

The bulk oxygen content of specimens manufactured in both the argon and argon-3% hydrogen atmosphere was analyzed to determine the effect of the shielding gas on oxygen content of the printed

specimens. Table II presents the oxygen content of pure molybdenum specimens printed in both conditions across a range of speeds. Given the affinity that molybdenum has for oxygen, the bulk oxygen content is assumed to be present primarily as molybdenum oxide. The specimens printed in the argon-3% hydrogen condition exhibited much higher oxygen content relative to those printed in pure argon. Additionally, there was strong sensitivity to laser scanning speed in the argon-3% hydrogen specimens, with slower speeds leading to higher oxygen content.

The oxygen content of the pristine Mo and Re powders as well as for each Mo-Re alloy printed in each atmosphere is presented in Table II. Similar to pure molybdenum, the Mo-Re specimens exhibited

Table II. Oxygen content of powders and printed compositions

Composition	Atmosphere	Scanning speed	Oxygen content
		(mm/s)	(ppm)
Molybdenum powder	—	—	180
Rhenium powder	—	—	2720
Pure Mo	Ar	200	421
Pure Mo	Ar-H2	200	1921
Pure Mo	Ar	400	434
Pure Mo	Ar-H2	400	1276
Pure Mo	Ar	1000	430
Pure Mo	Ar-H2	1000	1023
Mo-5%Re	Ar	400	653
Mo-5%Re	Ar-H2	400	2742
Mo-10%Re	Ar	400	645
Mo-10%Re	Ar-H2	400	2743
Mo-25%Re	Ar	400	1196
Mo-25%Re	Ar-H2	400	1946

increased oxygen content when printed in argon-3% hydrogen. The Mo-25wt.%Re composition demonstrated a smaller difference in oxygen between the two atmospheres compared to the alloys with 5 wt.% and 10 wt.% rhenium. The as-received rhenium powder has a dramatically higher oxygen content than the molybdenum powder, which may be due to the powder size and processing differences between the two suppliers. The high oxygen content in the rhenium powder led to a marked increase in the oxygen content of all the Mo-Re specimens compared to the pure molybdenum specimens. Mo-Re specimens printed using 400 mm/s laser scanning speed were analyzed via inert gas fusion, which prevented the observation of the effect of laser speed on the chemistry of Mo-Re specimens.

The observation of higher oxygen content in specimens printed in argon-3% hydrogen gas was noted in a previous study of additively manufactured pure tungsten. Kemnitz et al. proposed that the argon-3% hydrogen atmosphere promoted oxidation of tungsten while also preventing sublimation of oxides.¹⁶ Therefore, an increased content of partially reduced oxides remained in the material, which was evidenced by unique oxide structures observed on grain boundaries. It appears that a similar process is occurring in the current study. Molybdenum oxidation begins at temperatures in excess of 450°C.²¹ During industrial reduction, molybdenum oxide is reduced to pure Mo through a two-step process. MoO₃ is first reduced to MoO₂ by heating in a 700–800°C oven in hydrogen atmosphere, and MoO₂ is then further reduced to pure Mo at a higher temperature of 950°C–1000°C.²² The temperature achieved during the LPBF process is sufficient to melt molybdenum and is thus significantly > 450°C, which allows for ample oxidation of the material in both argon and argon-3% hydrogen conditions. The combination of the hydrogen-3% argon atmosphere and the high temperature of the

melt pool mimics the reducing condition found in industrial furnaces. However, during LPBF the material experiences a very localized heating followed by rapid cooling as the laser passes across the material. The elevated temperature is not maintained on the material surface long enough to reduce MoO₃ to pure Mo.

Molybdenum oxide sublimates at temperatures > 800°C, resulting in material loss.²¹ Sublimation is expected to proceed in the argon atmosphere; however, the reducing force of hydrogen in the argon-3% hydrogen atmosphere prevents oxide sublimation, which is proposed as one cause of the increased oxygen content in specimens printed in this atmosphere.

The increased oxygen presence appears to beneficially inhibit grain growth in the final material, as visualized by the etched surfaces in Fig. 3 and the inverse pole figure maps in Fig. 3d and e. Average grain size of the pure Mo printed in argon, 102.8 μm, was markedly larger than pure Mo printed in argon-3% hydrogen, 49.3 μm. The argon-3% hydrogen environment may allow for oxides to develop within the specimen as the melt pool moves; these oxides then contribute to grain refinement.

Micro-structural refinement was also noted with the addition of high amounts of rhenium. Mo-25wt.%Re resulted in an average grain size of 35.4 μm and 83 μm when printed in argon-3% hydrogen and argon, respectively. The columnar grain structure was preserved in the material, as is visualized in the etched surface in Fig. 3c and the IPF map in Fig. 3f.

The oxygen content of Mo-25wt.% Re specimens printed in argon-3% hydrogen was surprisingly lower than the 5 wt.% or 10 wt.% compositions. High amounts of rhenium may alter the interaction between molybdenum and the infiltrating oxygen.

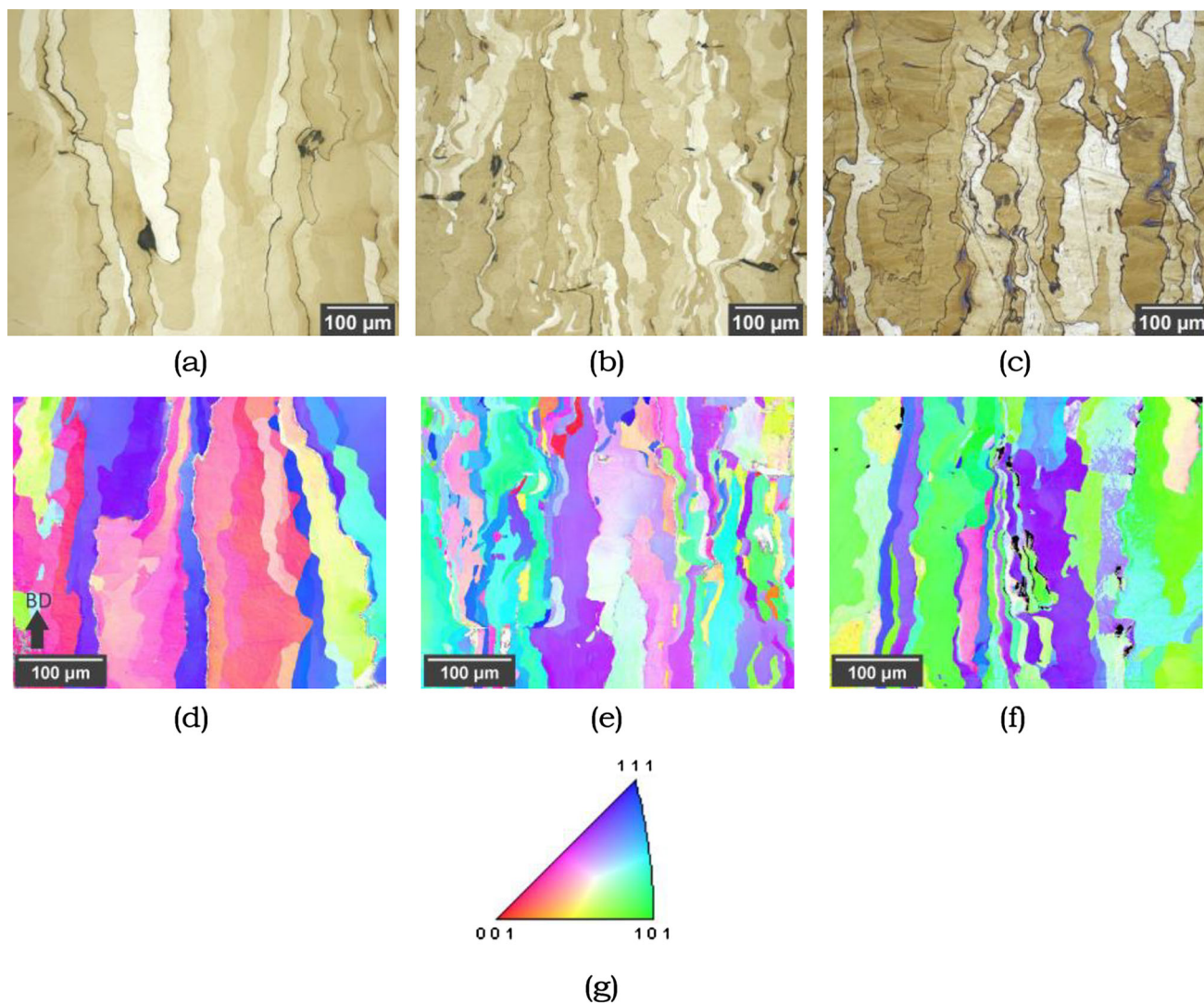


Fig. 3. Optical microscopy images of etched surfaces and EBSD maps of pure Mo printed in argon (a, d), argon-3% hydrogen (b,e), and Mo-25% Re printed in argon (c, f). Pole figure legend also shown (g). EBSD maps were taken in the XZ direction on specimens printed with 200 mm/s laser scanning speed.

Mechanical Testing

Molybdenum, like tungsten, is a brittle material prone to failure by intergranular fracture. Thermo-mechanical processing is commonly utilized in these metals during traditional manufacturing. Such a process greatly increases strength along the rolled or extruded axis of the material; however, this results in a large degree of anisotropy in mechanical properties between the longitudinal and transverse directions. A columnar microstructure, which is formed during manufacturing of some AM-produced materials,²³ gives rise to a similar degree of anisotropy between the build and transverse directions, which we refer to as vertical and horizontal. Across all of the strength results, the build direction had the largest effect on the flexural strength. Strength of vertically built specimens was much greater than for their horizontal counterparts, holding all other variables the same. Table III

shows the observed data, including mean strengths of horizontal and vertically built specimens across all compositions, in addition to the standard deviations. Coefficient of variation (COV), the dispersion of the strengths relative to their means, decreases dramatically for horizontal specimens as rhenium content is increased. Vertical specimens exhibit smaller COVs across all alloys.

Figure 4a displays a box plot of strength data relative to the alloy content (% Re), which shows a softening effect for Mo-5wt.%Re. Pure Mo has a median strength of 329 MPa, which dips down in Mo-5wt.%Re to 275 and begins to recover for Mo-10wt.%Re and Mo-25wt.%Re at 345 and 343 MPa, respectively. Mo-25wt.%Re has the highest strength with a lower standard deviation. Within the data is a variation of speeds among specimens (Fig. 4b), ranging from 200 to 1000 mm/s. Dispersion becomes higher at slower speeds for horizontal specimens

Table III. Descriptives of the observed data

Flexural strength (MPa)	Mean	Std dev	COV	Min	Max
<i>Horizontal</i>					
Pure Mo	149.3	90.0	0.60	55.9	272.3
Mo-5%Re	149.1	84.7	0.57	46.4	270.6
Mo-10%Re	162.3	64.0	0.39	76.9	270.0
Mo-25%Re	238.3	51.4	0.22	172.2	346.1
<i>Vertical</i>					
Pure Mo	554.5	141.0	0.25	254.6	798.2
Mo-5%Re	519.8	104.5	0.20	274.6	687.9
Mo-10%Re	563.0	75.8	0.14	345.1	658.5
Mo-25%Re	614.4	125.8	0.20	335.3	833.3

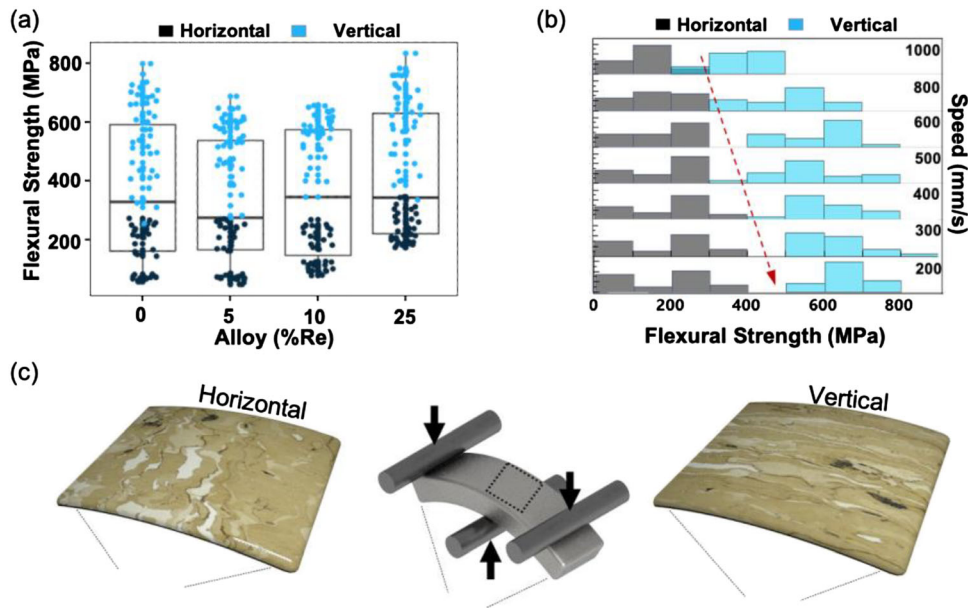


Fig. 4. (a) Box plot of the maximum strength data relative to the alloy concentration. Histogram of flexural strength relative to the (b) laser build speed shows an increase in strength at lower speeds. (c) Representation of the build direction grain structure shows how the elongated grains increase resistance to flexural loading. Data shown represent results from both build atmospheres.

but leads to strengths > 300 MPa. A trend of greater strength becomes apparent for vertical specimens as speed is decreased.

The sub-plots in Fig. 5 present the flexural strength of specimens printed with a horizontal build direction. Data are isolated relative to alloy content (Fig. 5a-d), with trend lines split according to build atmosphere. Processing in an argon environment hinders the strength of Mo-Re alloys relative to an argon-3% hydrogen atmosphere. The flexural strength of argon built specimens demonstrates a low sensitivity to the input laser scanning speed—a relatively flat (zero slope) strength profile is apparent across all speeds for all alloys. This finding indicates that a common microstructural feature is controlling the fracture mechanism regardless of laser energy in the argon specimens.

Processing in an argon-3% hydrogen atmosphere led to significant increases in flexural strength

($> 2 \times$), which can be seen as the H_2 data are translated upward on the strength axis relative to its argon gas counterpart. Unlike the pure argon atmosphere, a trend in strength relative to the laser scanning speed was observed in the argon-3% hydrogen atmosphere. Across all of the Mo-Re alloys, the strength is highest at the slowest laser speed (200 mm/s) and trends downward (negative slope) as the laser speed increases. The relationship between laser speed and strength can be explained by the oxygen concentration data of Table II. Oxygen concentration of the pure Mo specimens formed in argon-3% hydrogen was found to decrease as the laser speed increased. The hydrogen addition to the build atmosphere resulted in more oxides in the produced material, which act to strengthen the material. The highest relative strength for both printing environments was observed in the Mo-25%Re alloy. Increasing the rhenium content

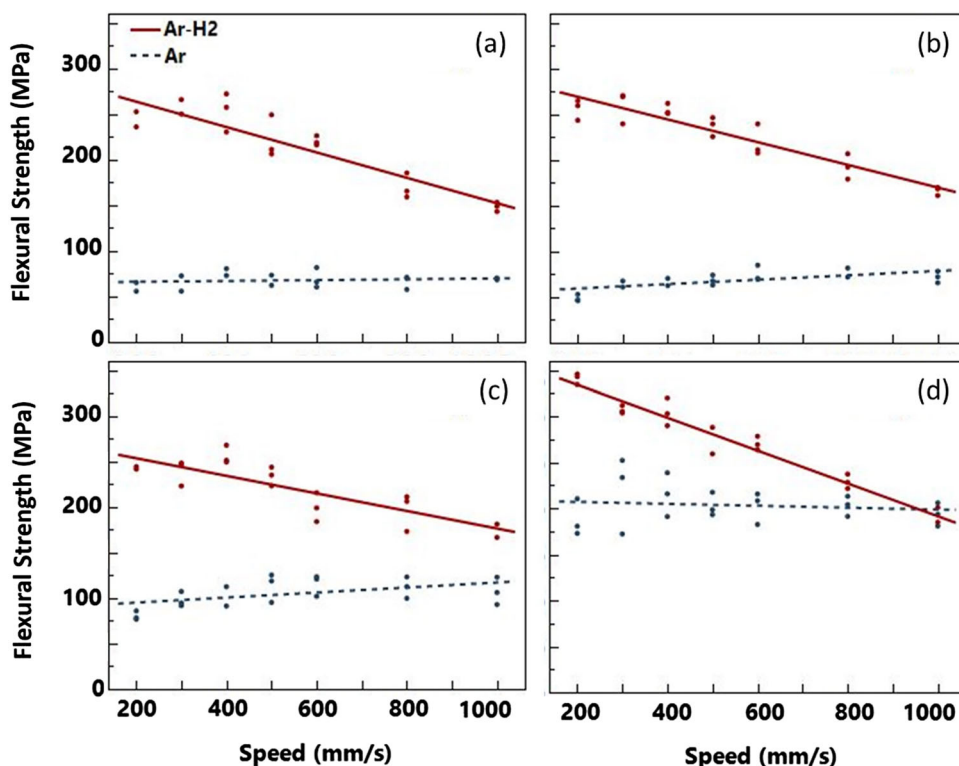


Fig. 5. The linear relationship of observed flexural strength regarding laser speed in the horizontal build direction for (a) pure Mo, (b) Mo-5%Re, (c) Mo-10%Re, and (d) Mo-25%Re.

appears to be an effective method to improve strength for the horizontal direction.

The sub-plots in Fig. 6 present the flexural strength of specimens printed with a vertical build direction. As mentioned previously, all specimens achieved an increased strength compared to those printed with a horizontal build direction because of the anisotropy inherent to the induced columnar microstructure. Similar to the behavior observed with the horizontal specimens, printing in argon-3% hydrogen led to increased strength, relative to the pure argon. As discussed, it is suggested that this strengthening effect is a result of the increased oxygen content in argon-3% hydrogen specimens. The oxygen impurity content may have helped pin grain boundary growth during processing resulting in the smaller grains. The refined microstructure of specimens printed in the hydrogen atmosphere leads to an increase in mechanical strength which may be due to a Hall-Petch effect or simply because the oxygen concentration is spread across a greater surface area than in the Ar specimens, thereby reducing the embrittling effects of oxygen even though its concentration is higher.

Specimens printed in the vertical build orientation demonstrated a sensitivity to the laser scanning speed in both processing conditions, with higher strengths being achieved at lower scanning speeds. The dependence on speed may be more evident in the vertical direction because of the fracture behavior. Horizontally printed specimens were broken with the force applied parallel to the columnar grains, promoting fracture primarily along grain boundaries which are weakly cohesive in the argon condition. By contrast, the vertically printed specimens were fractured with the force perpendicular to the columnar grains, requiring the crack to propagate through the grains during failure. A sufficient input of energy is required to manufacture dense parts, which is dependent upon the laser scanning speed. Porosity formed due to sub-optimal build parameters can serve as areas of crack initiation and stress concentration in the metal part, contributing to early failure of the built piece.

As can be noted in both Figs. 5 and 6, the addition of rhenium has a slight effect on the flexural strength of the specimens. The compositions with quantities < 25% rhenium behaved similarly to

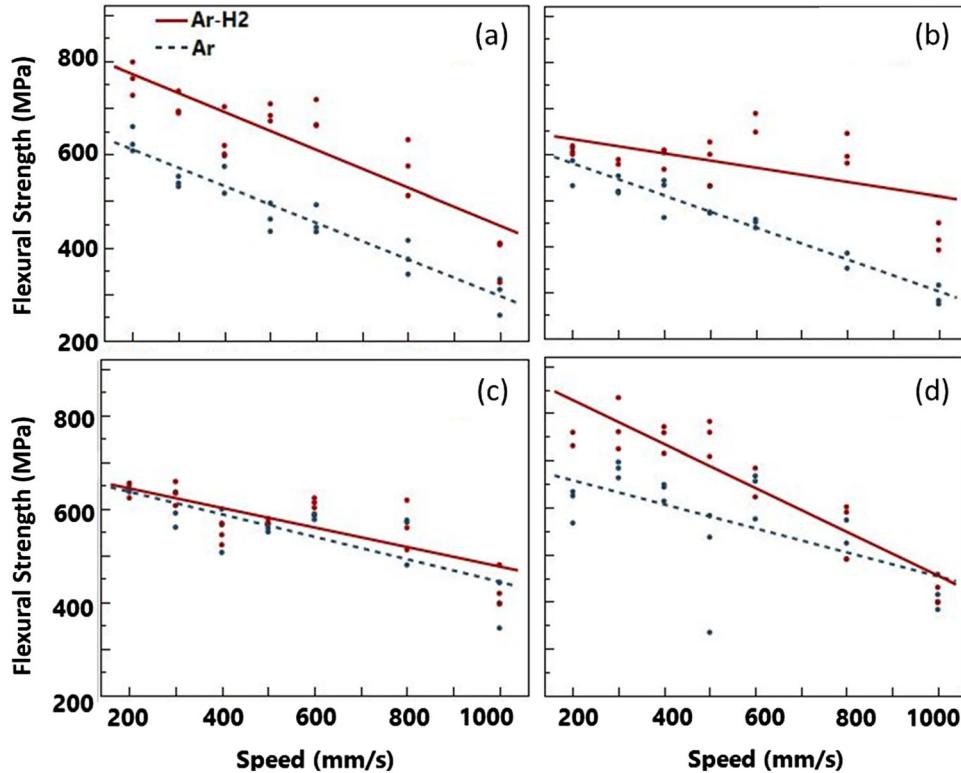


Fig. 6. The linear relationship of observed flexural strength regarding laser speed in the vertical build direction for (a) pure Mo, (b) Mo-5%Re, (c) Mo-10%Re, and (d) Mo-25%Re.

pure molybdenum. In the argon-3% hydrogen condition, there appears to be a softening effect. Many previous studies have demonstrated the phenomenon of small additions of rhenium decreasing the hardness and strength of molybdenum at low temperatures. The mechanism for this softening effect is still in question, but is commonly attributed to impurity scavenging.¹³ It is likely that the higher oxygen content of the samples printed in argon-3% hydrogen makes this softening effect more noticeable compared to the argon specimens where no decrease in strength at 5 or 10wt.%Re was noted.

Only the Mo-25%Re composition showed any improvement in flexural strength compared to the pure molybdenum, which was most notable at the slowest scanning speeds. While we begin to see the expected strengthening effect of rhenium in the Mo-25%Re compositions, additions closer to the solubility limit of 50wt.%Re may be necessary to achieve large-scale increases in strength.

Ductility has not been discussed thus far but it is worth noting that all specimens failed within or shortly after the linear-elastic region of mechanical behavior. This signifies that all specimens, regardless of grain size, oxygen content, or Re content,

failed in a brittle fashion. The brittle behavior may be a result of the high oxygen concentration or high strain energy induced by rapid heating and cooling during AM processing. Either case will inhibit dislocation motion during mechanical testing and result in higher strength values. Further studies involving post-processing heat treatments to reduce oxygen content and reduce strain energy would be worthwhile to highlight the strength of these effects.

Fracture Analysis

The microstructure generated by LPBF is dependent on the various processing parameters and strongly influences fracture behavior. Figure 7 is a set of SEM images of the fracture surfaces of pure Mo specimens after flexural testing. The figure presents a stark contrast of specimens with different process parameters. The horizontal specimens show features common to intergranular fracture in AM tungsten.¹⁶ Fracture surfaces of vertically built specimens exhibit river patterns indicative of transgranular fracture. This difference in fracture mechanism explains the large difference between the

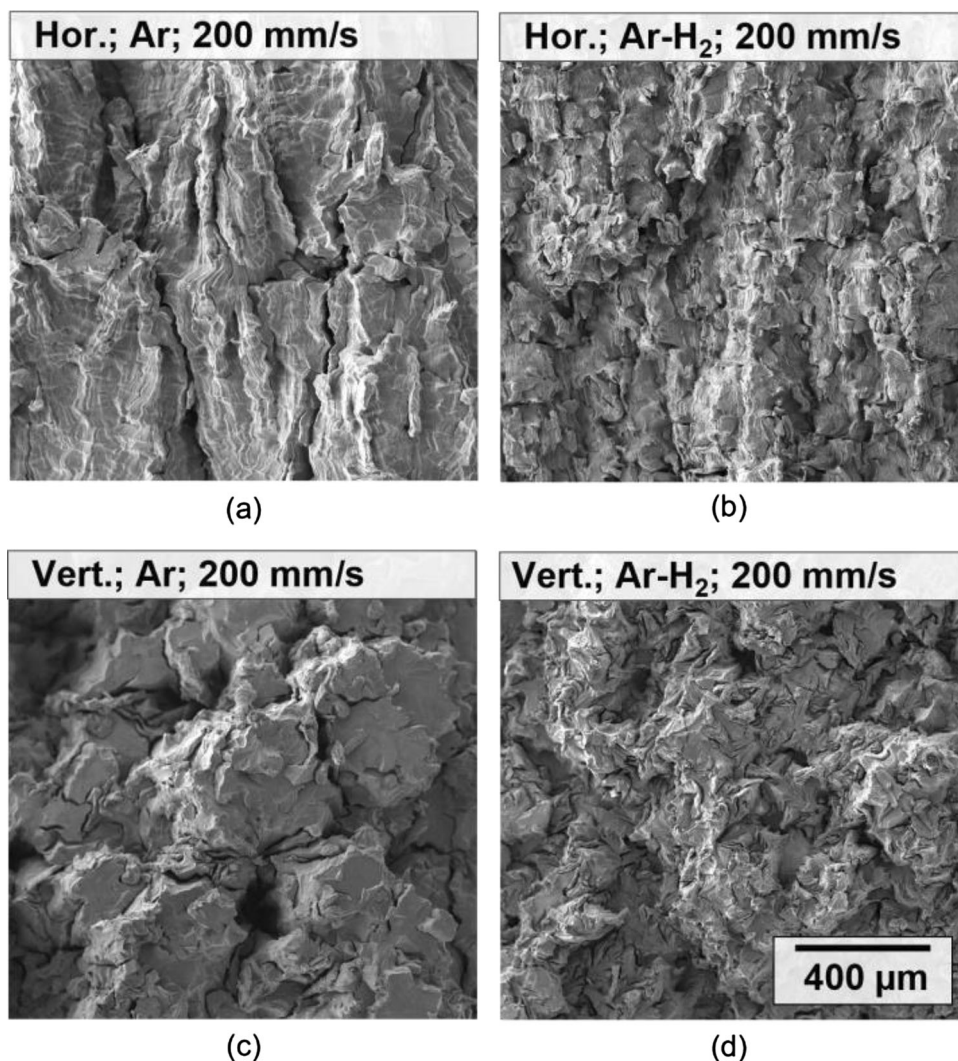


Fig. 7. Fracture surfaces of pure Mo specimens printed horizontally in argon (a) and argon–hydrogen (b); vertically in argon (c) and argon–hydrogen (d). The horizontal fractures surfaces predominately show intergranular fracture, whereas the vertical exhibit transgranular fracture.

flexural strength of horizontal and vertical specimens. A fracture surface travels more easily along the weakly cohesive grain boundaries of Mo than if the fracture has to travel through the grains.

The argon-3% hydrogen specimens show much smaller microstructural features on the fracture surfaces. Oxides were visible on the fracture surfaces of all compositions printed in argon-3%hydrogen, and representative images are displayed in Fig. 8. EDS in the SEM was used to investigate the composition of the oxides, but their small size and the uneven surfaces of the fracture surfaces make it difficult to accurately quantify the Mo, Re, and O content. The smaller grain sizes may be the driving force behind the strengthening effect noticed in both horizontal and vertical cases when printed with argon-3%hydrogen as it provides a larger grain

boundary area for oxygen to spread across and also forces the fracture surface to travel a more difficult path requiring greater fracture energy. The vertical argon-3% hydrogen specimens (Fig. 7d) also exhibit transgranular fracture, though the grains are much smaller than their argon counterparts and river patterns are more difficult to discern at the magnification shown.

The fracture surfaces of the Mo-25%Re specimens are shown in Fig. 9. The microstructural features appear even further refined than their pure Mo counterparts (Fig. 7), which is supported by EBSD and metallographic images presented previously. The smaller features contribute to the general strengthening effect according to a Hall–Petch relationship.

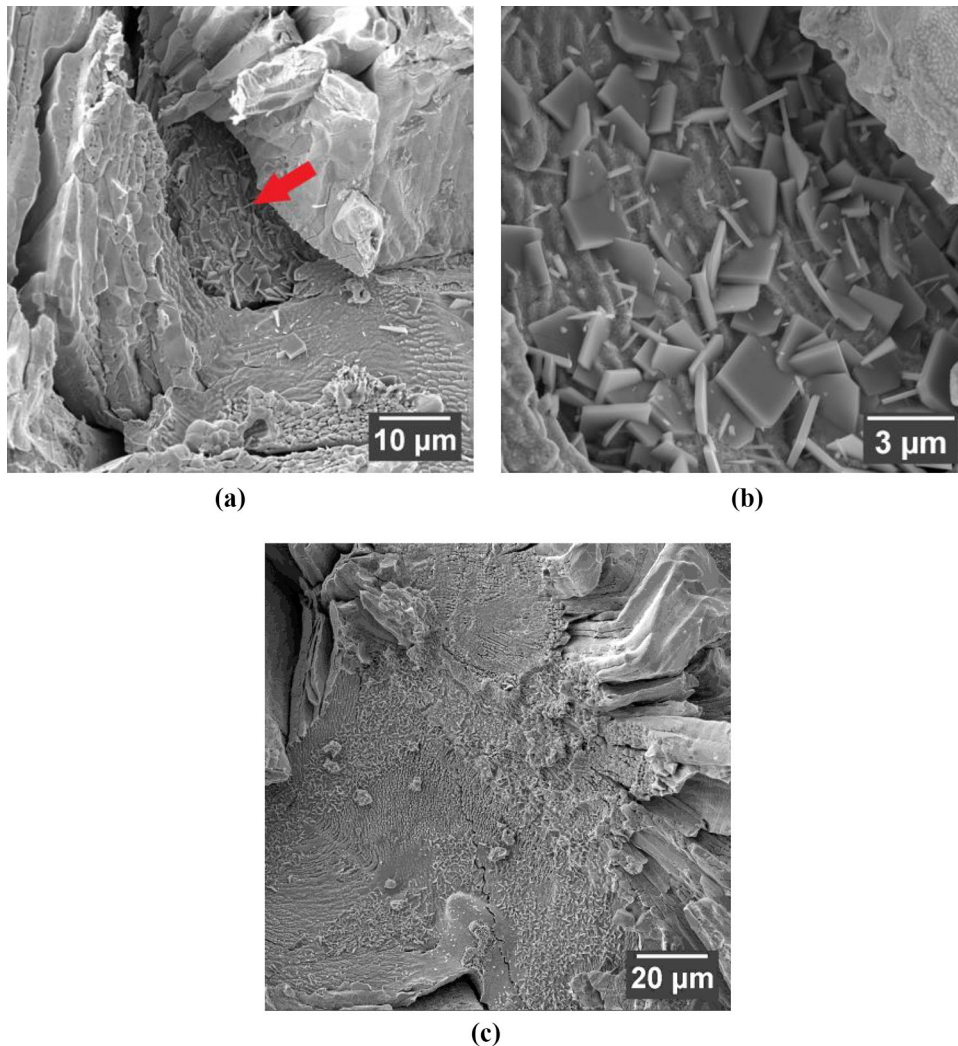


Fig. 8. Fracture surface of Mo-10Re. (a) High magnification of oxides from Mo-10Re (b) and fracture surface Mo-5Re (c). All specimens represented were printed in argon-3%hydrogen.

Additions of hydrogen to the shielding gas and rhenium to the alloy drive refinement of the microstructure, which greatly increases the grain boundary surface area. The increase in grain boundary surface area dilutes the concentration of impurities at the grain boundaries, thus promoting greater grain boundary cohesion and making it less favorable for cracks to propagate along them.⁹ The confounding piece of information is that the oxygen content tends to be higher in the hydrogen and high rhenium concentration cases, yet the net effect is still an increase in flexural strength. The combined benefit of reduced grain size and alloying content may offset the detrimental effect of oxygen impurities.

CONCLUSION

The low temperature mechanical performance of additively manufactured molybdenum alloyed with rhenium was investigated under varied processing conditions. Manufacturing under argon-3% hydrogen shielding gas led to a significant refinement of the grain structure of pure molybdenum and molybdenum rhenium alloys. The proposed mechanism is that the increased oxygen content in the bulk material beneficially inhibits grain growth.

Additions of rhenium below 25 wt.% provided a slight decrease in standard deviation among mechanical results, however no significant improvement in the mechanical performance of the

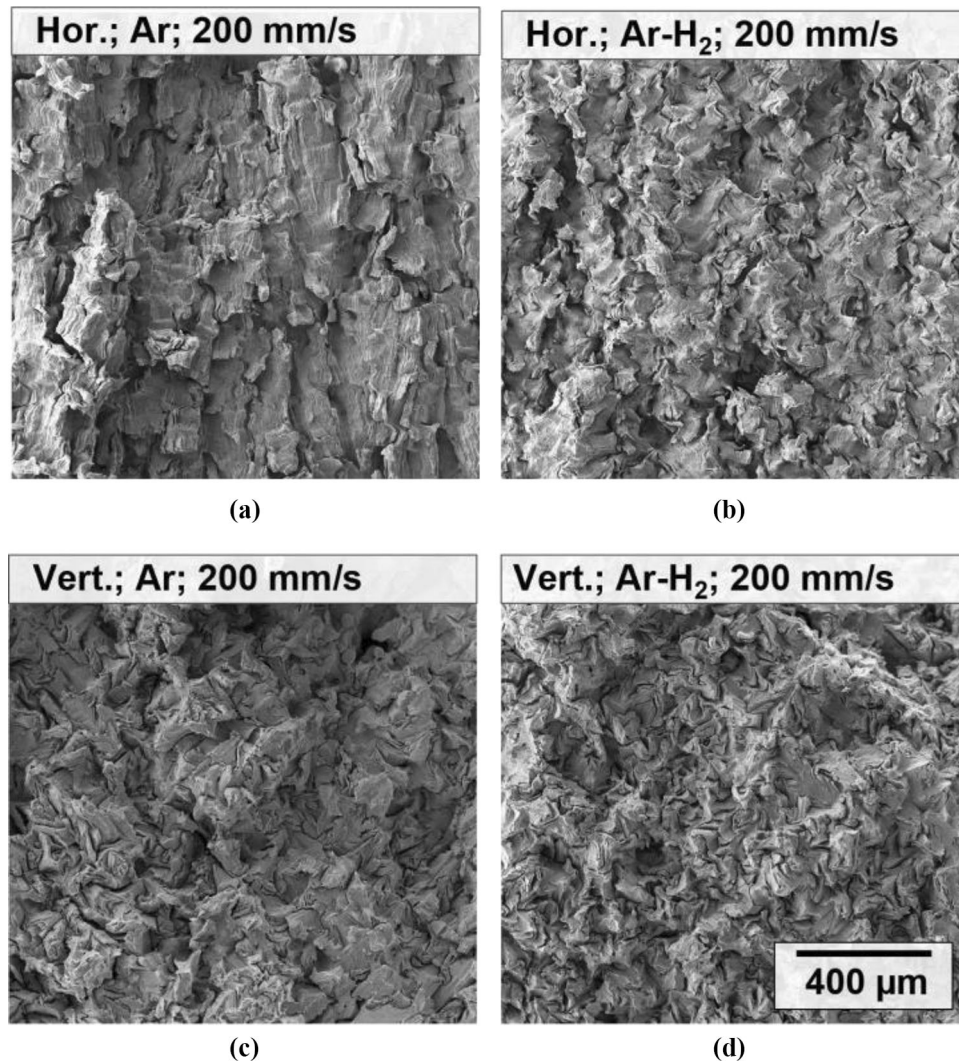


Fig. 9. Fracture surfaces of Mo-25Re specimens printed horizontally in (a) argon, (b) argon–hydrogen and vertically in (c) argon, (d) argon–hydrogen. Printed specimens tend to show more densely clustered grain sites with higher rhenium content, especially within a H₂ environment.

material. The 5% rhenium alloy appeared weaker than pure molybdenum, which is attributed to the rhenium softening effect.

CONFLICT OF INTEREST

On behalf of all authors, the corresponding author states that there is no conflict of interest.

ACKNOWLEDGEMENTS

This research was supported by the Materials and Manufacturing and Aerospace Systems directorates of the Air Force Research Laboratories.

DATA AVAILABILITY

The datasets generated and/or analyzed during the current study are available from the corresponding author upon reasonable request.

REFERENCES

1. J. Braun, L. Kaserer, J. Stajkovic, K.-H. Leitz, B. Tabernig, P. Stinger, P. Leibenguth, C. Gspan, H. Kestler, and G. Leichtfried, *Int. J. Refract. Hard Met.* 84, 104 (2019).
2. J. Braun, L. Kaserer, I. Letofsky-Papst, K.-H. Leitz, H. Kestler, and G. Leichtfried, *Int. J. Refract. Hard Met.* 92, 105 (2020).
3. L. Kaserer, J. Braun, J. Stajkovic, K.-H. Leitz, B. Tabernig, P. Singer, I. Letofsky-Papst, H. Kestler, and G. Leichtfried, *Int. J. Refract. Hard Met.* 84, 105 (2019).
4. L. Kaserer, J. Braun, J. Stajkovic, K.-H. Leitz, P. Singer, I. Letofsky-Papst, H. Kestler, and G. Leichtfried, *Int. J. Refract. Hard Met.* 93, 105 (2020).
5. M. Higashi, and T. Ozaki, *Mater. Des.* 191, 108 (2020).
6. P. Fernandez-Zelaia, C. Ledford, E.A. Ellis, Q. Campbell, A.M. Rosy, D.N. Leonard, and M.M. Kirka, *Mater. Des.* 207, 109 (2021).
7. J.B. Brosse, R. Fillit, and M. Biscondi, *Scr. Mater.* 15, 619 (1981).
8. M. Oku, S. Suzuki, H. Kurishita, and H. Yoshinaga, *Appl. Surf. Sci.* 26, 42 (1986).
9. T. Watanabe, and S. Tsunekawa, *Acta. Mater.* 47, 4171 (1999).

10. D. Faidel, D. Jonas, G. Natour, and W. Behr, *Addit. Manuf.* 8, 88 (2015).
11. T. Leonhardt, J.C. Carl'en, M. Buck C.R. Brinkman, W. Ren, C.O. Stevens, in Paper Presented at AIP Conference, American Institute of Physics, Maryland, 1999.
12. S.R. Agnew, and T. Leonhardt, *JOM* 55, 25 (2003).
13. J.R. Stephens, and W.R. Witzke, *J. Less-Common Met.* 23, 325 (1971).
14. P. Morcos, A. Elwany, I. Karaman, and R. Arr'oyave, *J. Mater. Sci.* 57, 9769 (2022).
15. X. Zhou, X. Liu, D. Zhang, Z. Shen, and W. Liu, *J. Mater. Process. Technol.* 222, 33 (2015).
16. R.A. Kemnitz, C.C. Eckley, B.M. Sexton, and A.R. LeSieur, *Int. J. Refract. Hard Met.* 110, 105970 (2022).
17. A. Durgutlu, *Mater. Des.* 25, 19 (2004).
18. M. Suban, J. Tüsek, and M. Uran, *J. Mater. Process. Technol.* 119, 193 (2001).
19. P. Kah, and J. Martikainen, *J. Adv. Manuf. Technol.* 64, 1411 (2013).
20. C. Yin, D. Terentyev, T. Zhang, S. Nogami, S. Antusch, C.-C. Chang, R.H. Petrov, and T. Pardoen, *Int. J. Refract. Hard Met.* 95, 105 (2021).
21. A.T. Nelson, E.S. Sooby, Y.-J. Kim, B. Cheng, and S.A. Maloy, *J. Nucl. Mater.* 448, 441 (2014).
22. E.R. Braithwaite and J. Haber, in *Molybdenum: An Outline of its Chemistry and Uses* (Elsevier, Amsterdam, Netherlands, 2013) pp. 20–25.
23. V.P. Sabelkin, G.R. Cobb, T.E. Shelton, M.N. Hartsfield, D.J. Newell, R.P. O'Hara, and R.A. Kemnitz, *Mater. Des.* 182, 108 (2019).

Publisher's Note Springer Nature remains neutral with regard to jurisdictional claims in published maps and institutional affiliations.